IOPscience iopscience.iop.org

Home Search Collections Journals About Contact us My IOPscience

Momentum and scalar transport in a localised synthetic turbulence in a channel flow with a short contraction

This content has been downloaded from IOPscience. Please scroll down to see the full text.

2011 J. Phys.: Conf. Ser. 318 052047

(http://iopscience.iop.org/1742-6596/318/5/052047)

View the table of contents for this issue, or go to the journal homepage for more

Download details:

IP Address: 84.6.221.229
This content was downloaded on 21/04/2015 at 14:01

Please note that terms and conditions apply.

Momentum and scalar transport in a localised synthetic turbulence in a channel flow with a short contraction

N. Lefeuvre[1], L. Djenidi[1] and S. Tardu[2]

[1] University of Newcastle, NSW Australia
[2] Laboratoire des Écoulements Géophysiques et Industriels (LEGI), Grenoble, France

E-mail: nathan.lefeuvre@uon.edu.au

Résumé.

A numerical simulation is undertaken to investigate the transport of momentum and a passive scalar in a localised turbulence in a channel with a contraction. The simulation is carried out using a hybrid method which combines the lattice Boltzmann method (LBM, for the velocity field) and the energy equation (for the temperature field). The localised turbulence is generated through pulsed jets issued in the Poiseuille flow developing in the channel at a Reynolds number of about 1000. The aim of the study is twofold : i) determine effect of the contraction on the localised turbulence, and ii) study how the passive scalar behaves in such contracted localised turbulence.

The contraction increase the averaged vorticity in the channel flow, which is accompanied by an increase in the averaged kinetic energy. The contraction also tends to reduce the Reynolds stresses. These results are similar those obtained in turbulent pipe flow with an axisymmetric contraction and in a turbulent boundary layer subjected to a favourable pressure gradient. However, it is found that the heat transport in the normal to the wall direction is more dramatically affected (reduced) than that in the direction of the flow.

1. Introduction

Mixing enhancement in a low Reynolds number in channel flows plays an important role in the development of relatively recent microfluidics systems, where the flow is almost always laminar (Glasgow & Aubry (2003) ; Wang *et al.* (2005)). Indeed mixing, which ultimately takes place at molecular level, is in large part controlled by the interface area between the components of streams contained in the mixture. Several techniques have been developed to increase the interface areas (Glasgow & Aubry (2003) ; Stroock *et al.* (2002)). Ideally, the interface area between two fluids, and thus the mixing, is optimized if some sort of chaotic motion can be generated in the laminar flow. The best way to enhance the mixing would to generate a turbulent-like localised region in an otherwise laminar base flow. Recently, Djenidi & Tardu (2010) showed that the use of two pulsed jets at the channel wall has the ability to generate localised "synthetic" turbulence in a Poiseuille flow at a subcritical Reynolds number of about 1000. Their work represented a practical application of a more theoretical study by Tardu *et al.* (2008) who showed that localised turbulence can be generated and eventually sustained through the interaction of two pairs of counter rotating longitudinal vortices. The use of the pulsed jets

Published under licence by IOP Publishing Ltd

by Djenidi & Tardu (2010) was motivated by the idea that such jets could generate two pairs of counter rotating vortices and thus lead to the generation of turbulence. These later authors found that the pairs of vortices created by the pulsed jets and the interaction of the jet heads with the upper wall generated a localised turbulence which interestingly has striking similarities with a fully developed turbulent channel flow. However, because the Reynolds number is relatively low, left alone the turbulence eventually decays under to the action of viscosity. One possible way to maintain the localised turbulence in the channel flow, without having to use several pairs of pulsed jets would be to mount a series of short contraction expansion in the channel geometry. The contraction would be used to accelerate the flow and intensify the vorticity and the expansion to help foster localised turbulence intensity with the view to maintain a turbulent region in the channel flow. It is known that, in the case of fully developed turbulent channel flow, the enhancement of streamwise stretching induced by contraction leads to the decrease of streamwise turbulent intensity in favour of cross stream fluctuations in the region away from the wall. The flow in the outer region tends to two component axial turbulence configuration dominated by wall normal and spanwise velocity fluctuations. The total turbulent kinetic energy increases near the wall, depending on the contraction ratio (Torbergsen & Krogstad (1998)). Similar result are observed in a turbulent boundary layer subjected to a favourable pressure gradient (Cal & Castillo (2008)). These aspects may have a positive impact on the development of localised spot in laminar base flow, and, to our knowledge, there is no reported study on this point.
The present paper reports a study on the behaviour of a localised synthetic turbulence generated by a pair of pulsed jets subjected to a contraction in a laminar channel flow. A direct numerical simulation based on a coupling of the lattice Boltzmann method and the energy equation is carried to compute the velocity and temperature fields.

2. Methods

2.1. lattice Boltzmann method

The velocity field is solved using the lattice Boltzmann method (LBM). The LBM is an alternative numerical approach to computational Fluid dynamic, which gained interest over the recent years. The basic idea of the LBM is to construct a simplified kinetic model that incorporates the essential physics of microscopic average properties, which obey the desired (macroscopic) Navier-Stokes equations (Frisch *et al.* (1986)). With a sufficient amount of symmetry of the lattice, the LBM implicitly solves these latter equations with second-order accuracy. For the present calculations, each computational node consists of a three dimensional lattice composed of 18 moving particles and a rest particle (lattice model D3Q19, for a developed account of LBM see Chen & Doolen (1998) ; Succi (2001)). The method was successfully used to simulate turbulent flows (Djenidi (2008) ; Djenidi (2006) ; Burattini *et al.* (2006)). In the present the standard lattice Boltzmann equation (LBE) with the Bhatnagar-Gross-Krook (BGK) is used.

2.2. Energy equation for thermal transport

The passive scalar, heat, is calculated with the use of the energy equation. The temperature is passive and do affect the velocity field. The behavior of the temperature is described by :

$$\frac{\partial \theta}{\partial t} + u.\nabla\theta = \frac{1}{Re.Pr}\nabla^2\theta \quad , \quad \theta = \frac{T - T_{cond}}{\Delta T} \tag{1}$$

where θ is the dimensionless temperature , T is the temperature and ΔT is the temperature difference between the top and bottom walls of the channel. The Runge-kutta 3rd order method

is used to discretize equation (1) and the matrix resolution is by the Crank-Nicholson method [Orlandi (2000)].

2.3. Computational domain and boundary condition

The three dimensional computational Cartesian domain (figure 1) has $30H \times 2H \times 4H$ mesh points in the stream-wise (x), normal to the wall (y), span-wise (z) directions and $H = 27$ (H is the half width of the channel. The mesh increments in the three directions are equal and regular. The bottom wall of the channel (5 mesh points of thickness) serves as a support for the jets. The orifices of the jets have a same size with 40 mesh points along x and 12 mesh points along z. They are shifted in spanwise direction by a distance of $\delta_z = 8$ mesh points on both sides of the centerline. The center of first orifice is located at $x = 2H$ and the second is shifted downstream by a distance $\delta_x = 20$ mesh points. Two channels are used in this study. The first one is a plane channel (CP) and the second is a plane channel with a contraction (CPC). In the CPC case, the contraction is located at $x = 12H$ jets. The ratio of contraction Cr is 1.26 (where $Cr = 2H/2H_2$, where H_2 is the half width of contracted channel section), thereafter noted CPC-1.26 . The flow is characterized by the Reynolds number, $Red = 1000$ (based on H and the bulk velocity) and the Prandlt number of 0.75. The pulsed jets are activated only once, i.e. only one pulse is triggered. At the jet inlet, i.e. $y = -1$, the velocity profile is imposed :

$$u_{t,x,y,z} = u_0 sin(\omega t) sin(\pi x) cos(\pi z) \tag{2}$$

where $\omega = \frac{2\pi}{T}$ and $0 < t < T$, with T is the period time, and $u_0 = 0.15$.
Periodic conditions are applied on the lateral sides (spanwise direction) of the domain and a zero gradient boundary condition is imposed at outlet. At the channel inlet, a parabolic velocity profile is applied. The maximum of velocity is obtained on the centreline and noted U_0. The lower and upper wall temperatures are at 1 and -1 respectively, and a linear temperature profile is set for the initial temperature field. The no-slip boundary conditions are applied at the walls though a bounce-back scheme.

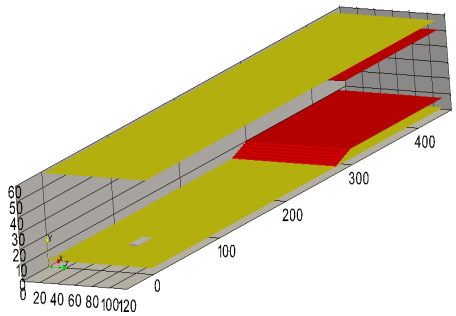


FIG. 1: Main channel with one jet (grey) in $x = 50$. The yellow correspond to wall of the plane channel (CP) and the red part correspond to the contraction (CPC-1.26).

3. Results

3.1. Space averaged kinetic energy

The time variation of the average turbulent kinetic energy and its components defined as follow :

$$E = \frac{1}{2}\frac{1}{E_{ini}}\int_V u^2 + v^2 + w^2 dV, \tag{3}$$

are shown in Figure 2 and 3, respectively. The integrations in expressions (3) are carried out over the turbulent region only, i.e. the localised turbulence. The difficulty for delimiting this region stems from the fact that this region not only travels downstream but its streamwise extent increases as well. To be able to define as best as possible a threshold based on the velocity component w was used. The threshold is set such that calculation of the energy are carried out if $w > 0.01E_{init}$. E is normalized by the average of the initial kinetic energy of the poiseuille flow. The energy reaches a maximum after the jets are activated (once only), decrease to a minimum at t^* of about 2.5 then increases to a maximum at t^* of about 5 then decreases over a long period before increasing again. Djenidi & Tardu (2010) associated this increase to possible turbulence regeneration. It seems that the contraction accentuates the increase of energy, suggesting it also

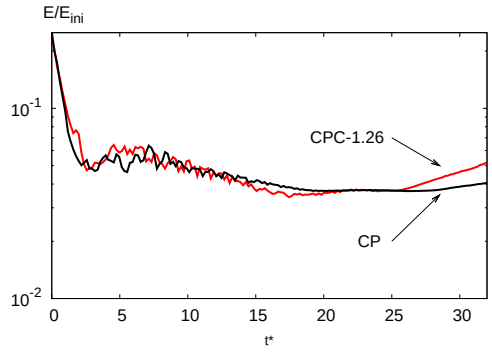


FIG. 2: Time variation of the average of the turbulent kinetic energy E for contraction (red) and without contraction (black). E is normalized by the average of the initial kinetic energy E_{ini}.

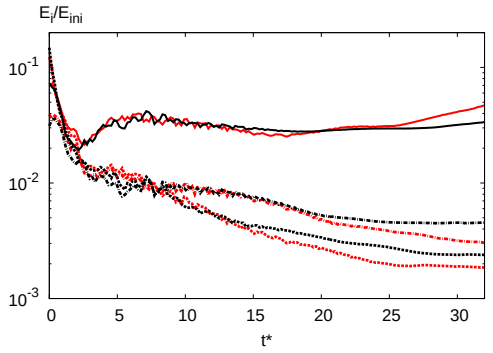


FIG. 3: Time variation of the components of the average of the turbulent kinetic energy for contraction (red) and without contraction (black). E_x (solid line), E_y (dash line) and E_z (dash-point line) are normalized by the average of the initial kinetic energy E_{ini}.

accentuates the process that takes naturally place even in the case without contraction, where a slight energy increase is observed. Indeed, while over the period $0 < t* < 15$ the energy with contraction behave similarly to that without contraction, it show some difference for larger t^*. This is better illustrated in Figure 3 which shows the three components of the energy. It is clear that the lateral components E_y and E_z in the case of contraction start to deviate from their no contraction counterparts at $t^* = 15$. Furthermore, E_x, the energy component along the streamwise direction, which is the principal contributor to total energy E for both cases, also starts its final increase (although weakly at first), at $t^* = 15$. The behaviour of the energy components indicates that $t^* = 15$ corresponds to the arrival of the pseudo-turbulent structure at the contraction. Figure 3 suggests that the contraction intensifies the "natural" mechanism that takes place in the channel and responsible for the slight energy increase observed in the no-contraction case. In particular, the rise of E_x and decrease of E_y and E_z are particularly accentuated reflecting a more intense energy transfer from the lateral components E_y and E_z to

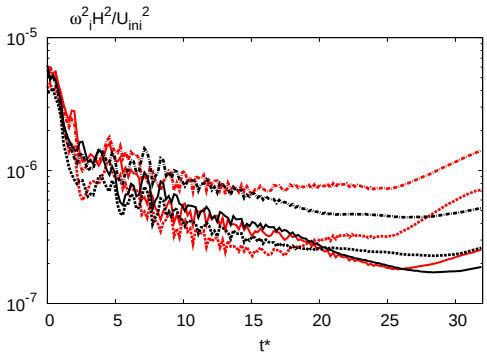


FIG. 4: Time variation of the average of squared vorticity components, for contraction (red) and without contraction (black). ω_x (solid line), ω_y (dash line), ω_z (dash-point line) are normalized by the average of the initial free stream velocity U_{ini} and the half-height H of the channel

the streamwise component E_x due to the contraction.
The effect of contraction on the pseudo-turbulent structure is also clear visible on the vorticity as seen in Figure 4 showing the three components , ω_x^2, ω_y^2, ω_z^2 of the enstrophy, ω^2 (ω is the vorticity magnitude). The three components with contraction depart significantly (they become bigger) from their no-contraction counterparts. Quite surprisingly, the longitudinal component ω_x^2 in the case of contraction deviates from the no-contraction distribution only for $t^* = 25$. This may suggest that this vorticity component responds with a delay to the contraction. Interestingly, the contraction seems to favour the development of the ω_y^2, ω_z^2 more than that of ω_x^2.

3.2. Velocity and temperature fluctuations

Figure 5 shows the turbulent intensity distributions u', v' and w' as function of y (the prime denotes rms values) at the instant $t^* = 30$. It is important to note that u_i' are calculated for each plan y within the domain $12H < x < 29H$. (12H represents the position of the contraction). At this instant the entire turbulent structure is within this domain. Note too that the same threshold as used in 3.1 is also used here. As seen previously (Djenidi & Tardu (2010)), the distributions present similar features to those observed in a fully developed turbulent channel

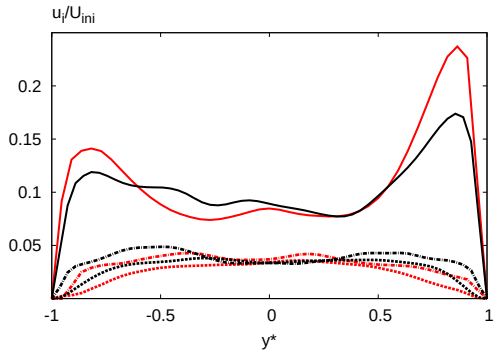


FIG. 5: Distributions along the direction normal-to the wall of the turbulent intensity components at $t^* = 30$ for contraction (red) and without contraction (black). u' (solid line), v' (dash line) and w' (dash-point line).

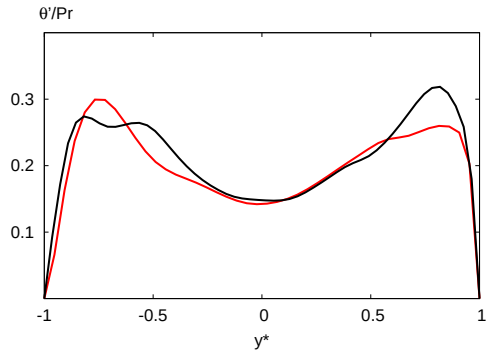


FIG. 6: Distributions along the direction normal-to the wall of the fluctuating part of the temperature θ' at $t^* = 30$ for contraction (red) and without contraction (black).

flow. However, the distributions are not symmetric with respect to centreline of the channel. Although the jets were issued at the bottom wall ($y^* = -1$), u'_{max} is larger in the upper region of the channel than in the lower region. This certainly reflects the strong interaction that took place between the head of the pulsed jets with the upper wall (see Djenidi & Tardu (2010)).
Relative to the no contraction case, the component u increases near the wall and reduced in the outer region, while the components v', w' show a rather opposite trend. Such behaviour is similar to that observed in the data of Torbergsen & Krogstad (1998) for a pipe flow with a contraction and Cal & Castillo (2008) for a turbulent boundary layer subjected to a favourable pressure gradient. Such behaviour is indicative of a relaminarisation process. However since the contraction is short and the turbulence in only localised and not fully developed it is not appropriate here to conclude to a relaminatization process. One can only argue that the localised turbulence present similar trends to a fully developed turbulence subjected to a contraction or favourable pressure gradient.
The temperature fluctuation rms is shown in Figure 6 for t* = 30 (the rms is normalised by

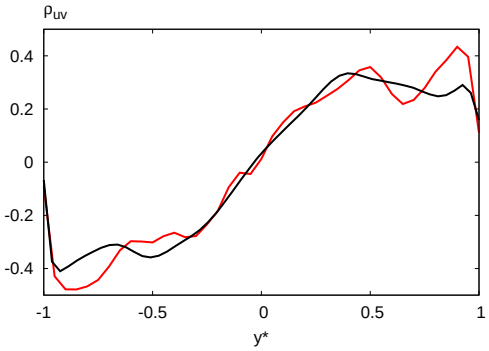


FIG. 7: Velocity coefficient correlation ρ_{uv} for contraction (red) and without contraction (black).

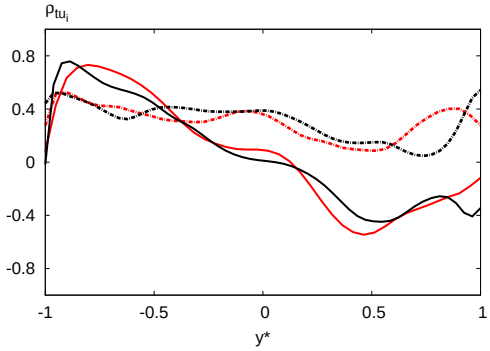


FIG. 8: Velocity-temperature coefficient correlation $\rho_{u_i\theta}$ for contraction (red) and without contraction (black). $-\overline{\theta u}/\theta' u'$: solid line ; $\overline{\theta v}/\theta' v'$: dash-point line.

the Prandtl number, Pr = 075). Like its velocity counterparts, the distributions of θ', for both cases, present striking similarities with the distributions of a heated fully developed turbulent channel flow. However, the contraction appears to affect θ' differently depending on the flow region. Near the upper wall θ' is reduced when compared to the case of no contraction, but it is increased near the lower wall. Such differences could reflect structural differences within the localised turbulence. This again may be explained by the different turbulence generation processes taking place at the lower and upper walls.
The contraction does not seem to affect dramatically the velocity coefficient correlation (Figure 7) or the velocity temperature coefficient correlation (Figure 8). However, it alters the distributions of uv , $u\theta$ and $v\theta$. (Figures 9 and 10 (10a and 10b)). The Reynolds shear stresses are reduced by the contraction away from the wall. Cal & Castillo (2008) showed that uv is decreases in a turbulent boundary layer when a favourable pressure gradient is applied. The similarity between the two results may not be too surprising because, although not shown here, the contraction induces a favourable pressure gradient. While the distribution of $u\theta$ with contraction does seem to differ dramatically from that without contraction, that of $v\theta$ with contraction departs markedly from that without contraction. This reflect that the transport of heat normal to the wall is more affect by the contraction than the heat transport in the direction the mean flow.

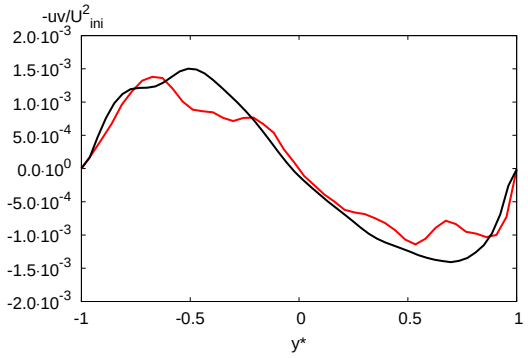
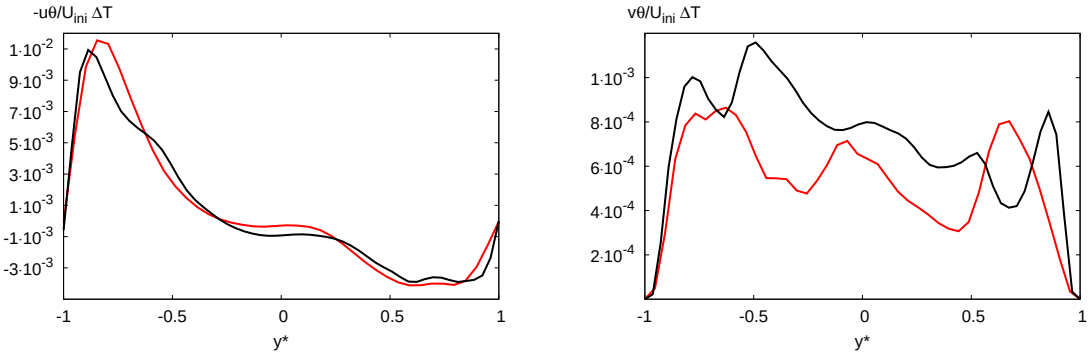


FIG. 9: Reynolds stress profiles $-uv$ for contraction (red) and without contraction (black). uv is normalized by the average of the initial velocity U_{ini}.



(a) (b)

FIG. 10: $u_i\theta$ for contraction (red) and without contraction (black). (10a) $-u\theta$ and (10b) $v\theta$ are normalized by the average of the initial velocity U_{ini} and ΔT.

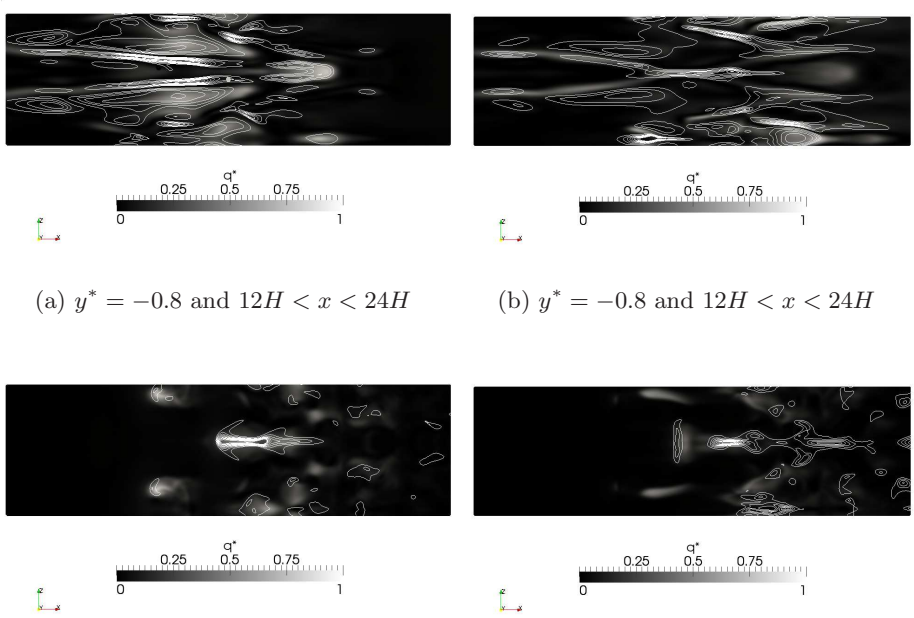
3.3. Flow visualization

The simulation results have been analysed in terms of flow visulaization. For example, figure 11 shows iso-contours of q^2 $(= u'^2 + v'^2 + w'^2)$ and θ^2. Each quantity is normalized by the its maximum value at the corresponding plane. Interestingly, a relatively good correlation between q^2 and θ^2 is reflected in the figure. This is reminiscent of the results of Antonia *et al.* (2009) who showed that θ^2 followed quite closely q^2 in a heated fully developed turbulent channel flow.

4. Conclusion

A direct numerical simulation based on a hybrid method combining the lattice Boltzmann method and energy equation was carried out to investigate the way a short contraction in a Poiseuille flow affects the velocity and temperature fields of a synthetic localised turbulence. The Reynolds number based on the channel height was about 1000 and the localised turbulence was generated by two pulsed jets at one wall of the two dimensional channel.
As compared to the case without contraction, the contraction tends to accentuate the mechanism responsible for the increase of the total kinetic energy in the channel flow as compared to the case without contraction. This may be explained by the observed increase in the total vorticity. The contraction, which generates a favourable pressure gradient, acts on the Reynolds stresses in a similar manner to that observed in a fully developed turbulent pipe flow with an axisymmetric contraction and in a turbulent boundary layer subjected to a favourable pressure gradient,

although less accentuated. The Reynolds stresses with contraction tend to be reduced away from the wall when compared to their no contraction counterparts.
It is also observed that the contraction affects the transport of heat in the normal direction more that in the mean flow direction.



(a) $y^* = -0.8$ and $12H < x < 24H$ (b) $y^* = -0.8$ and $12H < x < 24H$

(c) $y^* = 0$ and $12H < x < 24H$ (d) $y^* = 0$ and $12H < x < 24H$

FIG. 11: Instantaneous isocontours in the y-z plane of the turbulent kinetic energy q^2 and temperature variance θ^2 at $t^* = 30$ for CP (11a, 11c) and CPC-1.26 (11b, 11d). Isocontours are used for q^2. Lines are used for θ^2 ; the line increment is 0.1. The normalization is by the maximum value of q^2 and θ^2 for each plane.

Références

ANTONIA, R A, ABE, H & KAWAMURA, H 2009 Analogy between velocity and scalar fields in a turbulent channel flow. *J. Fluid. Mech* **628**, 241–268.

BURATTINI, P, LAVOIE, P, AGRAWAL, A, DJENIDI, L & ANTONIA, R A 2006 Power law of decaying homogeneous isotropic turbulence at low reynolds number. *PHYSICAL REVIEW E* **73**.

CAL, R B & CASTILLO, L 2008 Similarity analysis of favorable pressure gradient turbulent boundary layers with eventual quasilaminarization. *PHYSICS OF FLUIDS* **20**.

CHEN, S & DOOLEN, G D 1998 Lattice boltzmann method for fluid flows. *Annu. Rev. Fluid. Mech.* **30**, 329–364.

DJENIDI, L 2006 Lattice boltzmann simulation of a grid-generated turbulence. *J. Fluid Mech* **552**, 13–35.

DJENIDI, L 2008 Structure of a turbulent crossbar near-wake studied by means of lattice boltzmann simulation. *PHYSICAL REVIEW E* **77**.

Djenidi, L & Tardu, F S 2010 Localized turbulence generated by low energy pulsed jets in a laminar flow. In *ERCOFTAC*.

Frisch, U, Hasslacher, B & Pomeau, Y 1986 Lattice-gas automata for the navier-stokes equation. *PHYSICAL REVIEW LETTERS* **56**, 1505–1508.

Glasgow, Ian & Aubry, Nadine 2003 Enhancement of microfluidic mixing using time pulsing. *Lab Chip* **3**, 114–120.

Orlandi, P 2000 *Fluid Flow Phenomena : A Numerical Toolkit*. Kluwer Academy Publishers.

Stroock, A D, Dertinger, S K. W., Ajdari, A, Mezic, I, Stone, Howard A., & Whitesides, G M 2002 Chaotic mixer for microchannels. *Science* **295**, 647–651.

Succi, S 2001 *The lattice Boltzmann equation for fluid dynamics and beyond*. Oxford University Press.

Tardu, F S, Nacereddine, R & Doche, O 2008 An interactive bypass transition mechanism in wall-bounded flows. *J. Fluid Mech.* **615**, 345–369.

Torbergsen, L E & Krogstad, P A 1998 Axisymmetric contraction of fully developed pipe flow. In *13th Australasian Fluid Mechanics Conference, Melbourne*.

Wang, J, Wang, M & Li, Z 2005 Lattice boltzmann simulations of mixing enhancement by the electro-osmotic flow in microchannels. *Modern Physics Letters B,* **319**, 1515–1518.